PROCEEDINGS OF SPIE

SPIEDigitalLibrary.org/conference-proceedings-of-spie

Indices of polarimetric purity: application in biological tissues

Rodríguez, Carla, Van Eeckhout, Albert, Garcia-Caurel, Enrique, Gil, José, Garnatje, Teresa, et al.

Carla Rodríguez, Albert Van Eeckhout, Enrique Garcia-Caurel, José J. Gil, Teresa Garnatje, Emilio González-Arnay, Josep Vidal, Juan C. Escalera, Ignacio Moreno, Juan Campos, Angel Lizana, "Indices of polarimetric purity: application in biological tissues," Proc. SPIE 11646, Polarized Light and Optical Angular Momentum for Biomedical Diagnostics, 116460P (5 March 2021); doi: 10.1117/12.2578254

SPIE.

Event: SPIE BiOS, 2021, Online Only

Indices of Polarimetric Purity: application in biological tissues

Carla Rodríguez*[a], Albert Van Eeckout[a], Enrique Garcia-Caurel[b], José J. Gil[c], Teresa Garnatje[d], Emilio González-Arnay[e,f], Josep Vidal[a], Juan C. Escalera[a], Ignacio Moreno[g], Juan Campos[a], Angel Lizana[a]

[a]Grup d'Òptica, Physics Department, Universitat Autònoma de Barcelona, 08193, Bellaterra, Spain;
[b]LPICM, CNRS, Ecole polytechnique, Institut Polytechnique de Paris, 91120, Palaiseau, France;
[c]Universidad de Zaragoza, Pedro Cerbuna 12, 50009, Zaragoza, Spain;
[d]Botanical Institute of Barcelona (IBB, CSIC-ICUB), 08038, Barcelona, Spain;
[e]Departamento de Anatomía, Histología y Neurociencia, Universidad Autónoma de Madrid, 28049, Madrid, Spain;
[f]Servicio de Anatomía Patológica, Hospital Universitario de Canarias, 38320, Santa Cruz de Tenerife, Spain;
[g]Departamento de Ciencia de Materiales, Óptica y Tecnología Electrónica, Universidad Miguel Hernández de Elche, 03202, Elche, Spain;

*carla.rodriguez@uab.cat

ABSTRACT

Complete characterization of biological samples is of potential interest in different industrial and research areas, as for instance, in biomedical applications, for the recognition of organic structures or for the early detection of some diseases. During the last decades, polarimetric methods are experiencing an increase of attention in the study of biomedical tissues, and they are nowadays used in such framework to provide qualitative (polarimetric imaging) and quantitative (data processing) information for the studied samples. Polarimetric methods are based on the analysis of polarization modifications produced by light-matter interactions which can be triggered by a number of complex internal processes but can be roughly understood as the result of the combination of three pure polarimetric features of the sample: its diattenuation, retardance and depolarization. For the analysis of the depolarization content, we propose the use of the Indices of Polarimetric Purity (IPP) to describe the sample behavior. Related with the randomness of the scattering processes, IPPs provide more information of depolarizing systems than the widely used depolarization index (P_Δ), which further synthetize the depolarization content of samples. Moreover, certain combinations of IPP parameters leads to P_Δ. As a result, IPPs allow the revelation of some structures from tissue samples hidden in regular intensity images of even in the P_Δ channel, leading to better tissue classification results. In this work, we present different applications of IPPs in biomedical tissue that show its potential, which are not restricted to the biomedical framework as relevant results in plants characterization are also presented.

Keywords: Polarimetry, biological tissue, Mueller matrix, depolarization, imaging, biomedical, plants.

1. INTRODUCTION

Polarimetry comprises a set of non-invasive techniques [1] based on the measuring and comprehension of the different inherent polarized light-matter interaction properties of samples. These methods compound a very useful tool for its application in biomedical applications [2-6], for instance to early diagnose breast cancer [6] and skin cancer [7,8] among others [9], providing constitutive information of the biological structures of different tissues [10-14] and for curative processes [15-17]. Additionally, when looking for both quantitative and qualitative information of biological samples, an important polarimetric analysis is the so-called Polarization Gating (PG), which provides an enhance of the sample's intensity image contrast when using controlled polarized illumination channels [11].

In contrast with animal samples, botanical framework polarimetric studies (for instance, plant taxonomy [18] and vegetation classification [19]) are mostly based on the extraction of Degree of Polarization (DoP) [20,21] by measuring

Polarized Light and Optical Angular Momentum for Biomedical Diagnostics, edited by Jessica C. Ramella-Roman, Hui Ma, Tatiana Novikova, Proc. of SPIE Vol. 11646, 116460P · © 2021 SPIE · CCC code: 1605-7422/21/$21 · doi: 10.1117/12.2578254

scattered or transmitted light [19,22-29]: to determine hydric stress on plants [21], monitor crop growth [30] or to study plants photosynthesis [31-33]. Because the achieved enhancement on image contrast strongly depends on incident polarization (different sate of polarization, SoP, lead to different structure revelation and enhancement) we highlight the potential of MM measurements, as this matrix encodes the whole polarimetric information of the sample [18,29,31-35].

The so-called Indices of Polarimetric Purity (IPPs) have been reported in literature [36-38] as an alternative but more sophisticated method to analyze and understand depolarizing behavior of general samples: IPPs provide an easy physically-interpretable breakdown of MM-encoded depolarization mechanisms information and, consequently, they allow to classify different types of depolarizers. We recently demonstrate [3], by comparing covariance matrix eigenvalue-based [39] and canonical depolarizer parameters spaces [40,41], how IPPs purity space (which belongs to eigenvalues-based group) constitutes a potential biological tissue classifier.

By performing a complete polarimetric analysis of an *ex-vivo* chicken muscle sample and an *Epipremnum aureum* leaf, in this work we highlight the suitability and interest of including IPPs analysis as a useful tool when studying depolarization behavior of biological samples, both animal and vegetal. We show how they provide an overall enhance of image contrast focusing on different depolarizing nature structures and also unveil information which remains hidden if standard polarimetric indicators are used. Complementary, the mathematical background of depolarization metrics, and polarimetric instrumentation necessary to implement this method is also described in this work.

2. ENPOLARIZATION METRICS

In this section we review the different depolarization metrics we use for biological samples analysis. Particularly, we briefly introduce the most common Mueller matrix decomposition methods for the posterior extraction of depolarizing parameters, such as Indices of Polarimetric Purity (IPP).

The polarimetric characteristics of a sample are encoded into its Mueller matrix (MM) in a complex way [20,21,36,37,48-51], but three mainly physical characteristics can be retrieved: diattenuation-polarizance, retardance and depolarization. Particularly, we review some of the mathematical expressions related with the enpolarization (polarization and depolarization) mechanism of samples, which have proved to be useful in the context of biological samples analysis. We start by defining the 4x4 MM by means of physically known elements [20]:

$$\hat{M} = M / m_{00} = \begin{pmatrix} 1 & D^T \\ P & m \end{pmatrix} \tag{1}$$

$$\vec{D} = (m_{01}, m_{02}, m_{03})^T \quad , \quad \vec{P} = (m_{10}, m_{20}, m_{30})^T \tag{2}$$

being m_{00} the mean MM intensity, **P** the polarizance and **D** the diattenuation vectors (whose absolute values are P=|**P**| and D=|**D**|, respectively). Whereas the polarizance, P, gives a measure of the capability of the sample to polarize a fully unpolarized input state, the diattenuation, D, completely describes the transmittance dependence of the sample with the input polarization state.

Additionally, the total retardance, R, which magnitudes the retardance behavior of the sample, can be computed [20]. To do so, the Lu-Chipman decomposition [20] is the most commonly used approach: it synthetizes the polarimetric information of **M** in a product of three pure MMs, which are function of well-defined polarimetric magnitudes:

$$M = M_\Delta M_R M_D \tag{3}$$

being M_Δ, M_R and M_D the pure depolarizer, retarder and diattenuator, respectively. From M_R we get the expression for retardance, R:

$$M_R = \begin{pmatrix} 1 & \vec{0}^T \\ \vec{0} & m_R \end{pmatrix} \quad , \quad R = \cos^{-1}\left(\frac{tr(m_R) - 1}{2} \right) \tag{4}$$

Finally, to study the depolarizing properties of the sample, the Cloude's decomposition [48] can be applied, which defines a general Mueller matrix **M** as a parallel combination (convex sum) of four pure MMs ($\hat{M}_{Ji}$) with different weights proportional to covariance matrix **H** eigenvalues ($\hat{\lambda}_i$) [20,52]:

$$M = m_{00} \sum_{i=1}^{4} \hat{\lambda}_i \hat{M}_{Ji} \tag{5}$$

Above-mentioned eigenvalues are restricted to a range from 0 to 1 (the sum of all eigenvalues is m_{00} so the normalized eigenvalues are not completely independent) and fulfill $\lambda_1 \geq \lambda_2 \geq \lambda_3 \geq \lambda_4 \geq 0$. By combining the normalized covariance matrix eigenvalues, we obtain three real, invariant and dimensionless parameters defined as indices of polarimetric purity (IPP) [48]:

$$P_1 \equiv \hat{\lambda}_1 - \hat{\lambda}_2, \qquad P_2 \equiv \hat{\lambda}_1 + \hat{\lambda}_2 - 2\hat{\lambda}_3, \qquad P_3 \equiv \hat{\lambda}_1 + \hat{\lambda}_2 + \hat{\lambda}_3 - 3\hat{\lambda}_4 \tag{6}$$

which fulfill $0 \leq P_1 \leq P_2 \leq P_3 \leq 1$. These IPPs provides the randomness introduced by samples and are an ideal framework to study depolarizing media [2,3,18,54].

Additionally, the well-known depolarization index, P_Δ, can be related with IPPs in the following way:

$$P_\Delta = \frac{1}{\sqrt{3}} \sqrt{2P_1^2 + \frac{2}{3}P_2^2 + \frac{1}{3}P_3^2} \qquad 0 \leq P_\Delta \leq 1 \tag{7}$$

These indicators characterize a pure (non-depolarizing, $P_\Delta = 1$) system when $P_1 = P_2 = P_3 = 1$. Otherwise, an ideal depolarizer ($P_\Delta = 0$) is described for $P_1 = P_2 = P_3 = 0$. The P_Δ indicator provides an overall measure of depolarization, and it is suitable for a homogeneous depolarization, but if there is a dependence of the degree of depolarization introduced by a sample with the input polarization, the IPPs metrics are a more appropriate election.

3. METHODOLOGY

In this section we present a complete characterization of the image Mueller polarimeter used for samples characterization, and include a brief description of the samples studied (both *ex-vivo* animal tissues and plants).

3.1 Complete image Mueller polarimeter

The acquisition of experimental Mueller matrices of the different biological samples is performed by means of a complete image Mueller polarimeter (Fig. 1) based on Parallel Aligned Liquid Crystals (PA-LC) retarders. It consists of two compact and mobile arms: The Polarization State Generator (PSG), which is composed by a linear polarizer oriented at 0º, followed by two PA-LC at 45º and 0º, respectively, with respect to the laboratory vertical, and the Polarization State Analyzer (PSA), whose internal elements are the same as those in PSG but arranged in the inverse order. The final sample's intensity image is captured by means of a CCD camera. This PSG-PSA scheme is capable to generate any fully polarized state of polarization and to detect any polarization (fully polarized, partial polarized or depolarized) [41]. We usually conduct two different optical configuration measurements: i.e. (1) scattering configuration (by modifying the incident angle by tilting the PSG with respect to the optical table – we usually use an incident angle of 56º – and maintaining PSA at 0º in order to avoid the ballistic reflection); and (2) transmission configuration (by placing both PSG and PSA at 90º). In addition, different illuminating wavelengths are also used, covering the visible range (625 nm, 530 nm and 470 nm), this allowing us to inspect different depths into the sample [55]. To build the experimental Mueller matrix, 36 images of the region of interest (1.1 × 1.1 cm^2) are taken in order to minimize the measurement noise (at least 16 images are needed): we use the 6 illumination (generators) states of polarization and the 6 analyzers proposed in [41]. Complete Mueller matrix measurement lasts approximately 3.6 seconds, considering the time of calculation of the Mueller matrix by using the inverse method (0.4 to 2.2 s) [20,21,56], PA-LC molecules orientation process from one polarization state to the following one (~ 100 ms) and CCD exposure time.

Particularly, the illumination is performed by means of a four-wavelength high-power Thorlabs LED source (LED4D211, operated by DC4104 drivers distributed by Thorlabs) complemented with 10nm dielectric bandwidth filters distributed by Thorlabs: FB530-10 and FB470-10 for green and blue wavelengths, respectively. About the linear polarizers: the one arranged on PSG is a Glan-Thompson prism-based CASIX meanwhile the one in PSA is a dichroic sheet polarizer

distributed by Meadowlark Optics. The four Parallel Aligned Liquid Crystals are Variable Retarders with Temperature Control (LVR-200-400-700-1LTSC distributed by Meadowlark Optics). Imaging is performed by means of a 35mm focal length Edmund Optics TECHSPEC® high-resolution objective followed by an Allied Vision Manta G-504B CCD camera, with 5 Megapixel GigE Vision and Sony ICX655 CCD sensor, 2452(H) × 2056(V) resolution and cell size of 3.45 µm × 3.45 µm, so a spatial resolution of 22 µm is achieved.

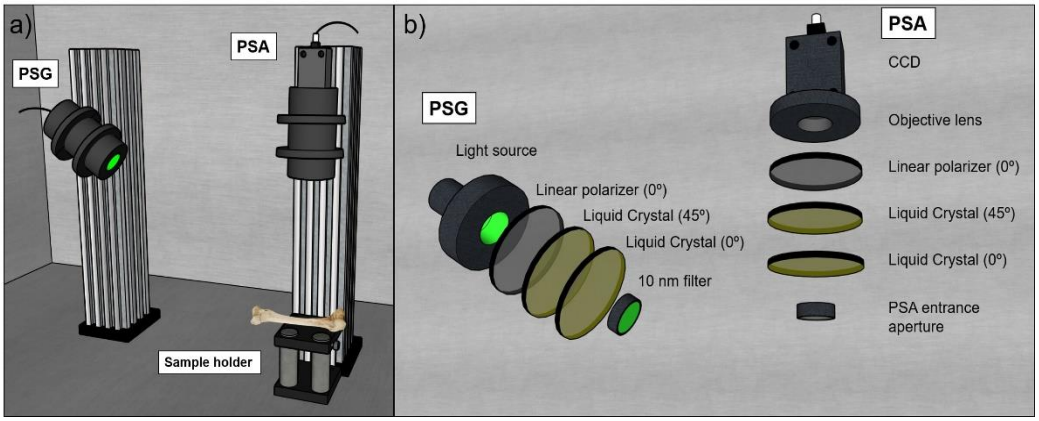

Figure 1. (a) General 3D representation of the complete image Mueller polarimeter used in this work, (b) closer and detailed 3D representation of Polarization State Generator (PSG) and Polarization State Analyzer (PSA) and their constituent optical components.

3.2 Samples description

The samples used for the polarimetric analysis are well differentiated into two groups: for the inspection of *ex-vivo* animal tissues, 20 different chicken thighs [53,54] were dissected and split into soft tissues. Particularly, 40 tendons, 40 muscles and 40 myotendinous junction were obtained and subsequently frozen at -16ºC. To work with the same decomposition conditions, chicken samples were systematically defrosted three hours before measured. Mentioned soft tissues present different physiological function and structural properties: tendon is composed by dense type-I collagen fibers (up to 60-80%) disposed, by following the same orientation as muscle bundles, in parallel and compact fascicles [57,58]. Skeletal muscle comprises bundled fascicles of contractile myofibrils chains (in counterpart to tendon, whose non-contractile properties allow it to withstand tensions) sheathed with type-I collagen rich tissues [59] which protect muscle fibers from friction. Myotendinous junction is a combination of the previously mentioned muscle and tendon tissues: fiber fascicles of contractile myofibrils and collagen are progressively mixed and covered by fasciae [60-62].

For the performance of other works [2,54] a trachea, heart and kidney of a suckling lamb and rabbit leg soft tissues and bone were studied. Particularly, trachea composition is based on hyaline cartilages rings (collagen type-II and chondroitin sulphate rich) covered and joined by annular ligament (collagen type-I and fibroblast cells rich fibrous membrane). Heart study was focused on an endocardial view, particularly on endocardium-covered muscle and sub-valvular apparatus on connective tissue. Undissected kidney was covered with fibrous capsule.

In counterpart to animal study, the polarimetric inspection in botanical framework is carried out by using an *Epipremnum aureum* (Linden & André) G.S. Bunting (Araceae) leaf, most commonly known as *Pothos aureus*. Native from Southeast Asia and New Guinea, this climbing plant is typically cultivated for decorative purposes. An herbarium voucher of *Pothos aureus* is deposited in the Herbarium of the Botanical Institute of Barcelona (BC843412). Because of the suitability of this polarimetric methods, we recently performed a similar study by using a *Hedera marocanna* McAll. leaf [18] even though this behavior has been tested and observed in different plant specimens such as *Prunus dulcis* (Mill.) D.A. Webb and *Spathiphyllum* sp.

4. RESULTS AND DISCUSSION

In this section we perform a complete polarimetric analysis of two well-differentiated biological groups: on one hand, we measure the MM of three distinct *ex-vivo* chicken soft tissues (tendon, muscle and myotendinous junction), obtained from a collection of 20 different chicken leg sections, at scattering configuration. Because of different wavelengths provide

different penetration lengths [55] these measurements have been repeated by using three distinct illumination channels (625 nm, 530 nm and 470 nm), covering the visible range. To not extend the work, we focus on presenting the results of muscle measurements but the same analysis on remain soft-tissues lead to similar conclusions. On the other hand, to complement animal tissue study, we conducted a transmission configuration MM measurement of an *Epipremnun aureum* leaf at 530 nm. The polarimetric analysis is the same for both groups: once we obtain the experimental MM, we extract, by means of matrix analysis introduced in Section 2, the associated depolarizing metrics (P_Δ and IPPs) as well as the intensity (m_{00}), diattenuation (D), and the retardance (R). For the sake of comparison with the qualitative analysis, we compute the visibility for different regions of interest (ROI) where hidden structures arise. The depolarizing metrics demonstrate an enhance of the image contrast when compared with regular intensity images. Moreover, we perform a pseudo-colored treatment [2] based on linear combinations of IPPs that leads to an enhancement of the visual contrast. Consequently, we highlight how IPPs synthetize, magnify and further characterize the overall depolarizing information inherent to the studied samples leading to an enhance of image contrast and the revelation of biological tissue structures that remain hidden when processed with standard methods.

4.1 IPP-based image contrast enhancement of ex-vivo chicken muscle sample

A discussion of the obtained results from chicken analysis is provided down below. As previously mentioned, the MM of the tissue is obtained at scattering configuration by illuminating at three main visible spectrum wavelengths: 625 nm, 530 nm and 470 nm. A region of interest (ROI) of 512 × 512 pixels (1.1 × 1.1 cm^2) is selected from the whole sample. By analyzing the output images from MM-metrics extraction (IPPs, R, D, and P_Δ) we point out, in agreement with many previous studies: i) retardance and depolarization constitute the polarimetric channels which provide the most significant amount of information [4,5,10-14, 22-24,42-47] in comparison with diattenuation and ii) blue wavelength illumination is appropriate when looking for surface details inspection [55]. Consequently, we choose the 470 nm channel to carry out the particular qualitative and quantitative analysis described in this proceeding.

Regular intensity image (irradiance response of the tissue against any incident state of polarization), given by m_{00}, of chicken muscle is shown in Fig. 2 (a). Standard MM-metrics (retardance R and depolarizing index P_Δ) images are given in Fig. 2 (b) and Fig. 2 (c), respectively. The diattenuation (D) image is not included because its response is not significant.

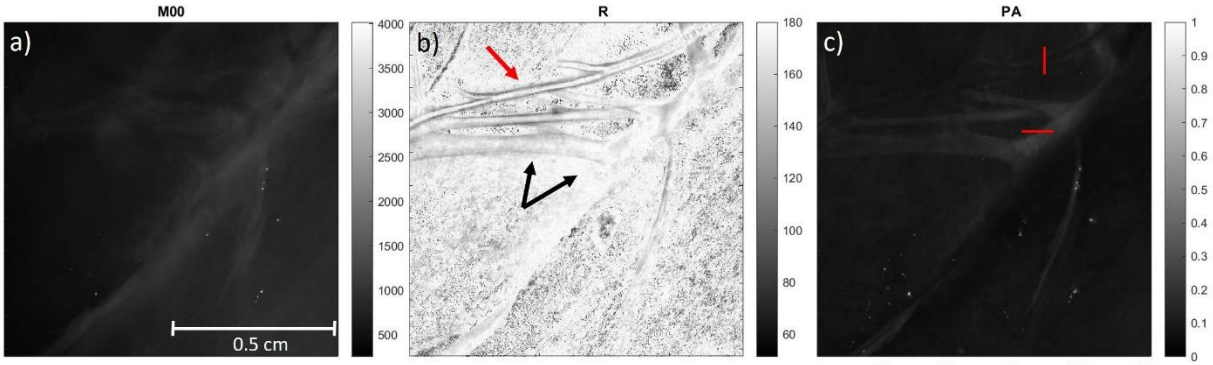

Figure 2. Standard MM-metrics extraction for polarimetric analysis of an *ex-vivo* chicken muscle sample. (a) Regular intensity image (m_{00}); (b) total retardance, R and (c) depolarization index, P_Δ. Red and black arrows indicate the presence of blood vessels and nervous tissue, respectively. Red lines correspond to two structures of interest in the sample.

Figure 2 shows the comparison between regular intensity image (Fig. 2(a)) and polarimetric-based ones (Figs. 2(b), 2(c)). Retardance response is spatial-dependent, as collagen-rich tissues induce birefringence to the incident polarization. This sample corresponds to a skeletal muscle pierced by a neurovascular bundle (both red and black arrows). The structures exposed by high birefringence behavior are the peripheral nerve (black arrows in Fig. 2(b)) and the blood vessel walls (red arrow in Fig. 2(b)), with an inner (*tunica intima*) layer rich in elastic fibers and a middle layer composed mainly by smooth muscle cells. In turn, depolarization response (P_Δ) reveals the presence of the same structures. In this context, we can assume that those biological tissues are composed by scattering units whose density and size are different from those in a skeletal muscle belly (contractile myofibril chains uniformly arranged). Taking special attention to depolarization index gray scale we find that collagen-rich structures of the neurovascular bundle are more non-depolarizing (larger P_Δ values) than regular muscle (low P_Δ). This is consistent with the previous statement: the nerve is mainly composed by fascicles densely packed in concentric sheaths of collagen (epineurium, perineurium, endoneurium) that produce high birefringence

behavior and constitute a low depolarizing mechanism. In contrast, the response of the vascular structures and the skeletal muscle is more depolarizing: the scattering produced by blood and hydration in muscle is typically higher than in collagen-rich tissues. This fundamental composition difference leads to an enhance on image contrast when analyzing the depolarization behavior of the sample.

To highlight the convenience of the use of indices of polarimetric purity (IPP) when performing a polarimetric study of a biological tissue sample, we analyze the behavior of isolated P_1, P_2 and P_3. Obtained results are presented in Fig. 3. When comparing the response of IPPs with the standard MM-metrics in Fig. 2, an enhancement on image contrast is clearly observable. This is consistent with the fact that depolarization index is related with IPPs by a weighted average of them [48]: the information P_Δ provides is decoded and synthetized into three indicators related with the inherent depolarizing mechanisms and, consequently, one of these particulars should enhance the contrast between different sample structures. Down to the last detail, P_1 strongly magnifies large collagen-rich structures. Additionally, P_2 slightly unwraps hidden information (red arrows) while continues enhancing the overall image contrast. Finally, P_3 may blur the strong delimitation provided by P_1 but new structures arise (yellow arrows). The study of isolated IPPs manifest differences in the depolarizing capability of the different tissue regions (in turn, biological compositions) not seen by commonly-used depolarization metrics: recalling the weight of each purity component contribution on the whole depolarization index P_Δ (Eq. (7)), the new structures revelation (mainly produced in P_3 and P_2) is shielded by P_1 because of the largest contribution from the last.

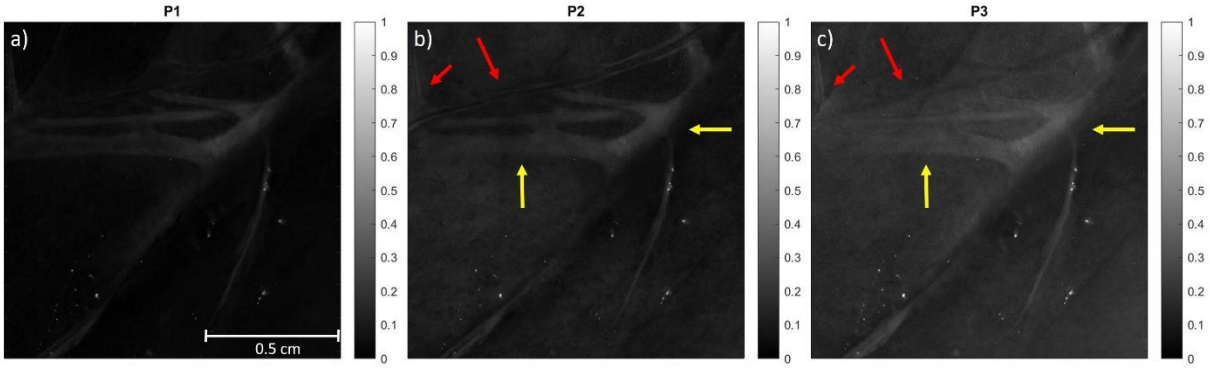

Figure 3. Indices of polarimetric purity images for polarimetric analysis of an *ex-vivo* chicken muscle sample. Red and yellow arrows indicate the revealed blood vessels and nervous tissue, respectively. (a) P_1; (b) P_2 and (c) P_3 images.

Supplementary to the qualitative analysis of polarimetric study, we compute the visibility (Vis) of the red-lined regions of interest (ROI of 1×40 pixel) in Fig. 2 (c), by selecting the respective highest (I_{max}) and lowest (I_{min}) values of the whole ROI pixels for depolarization indicators (P_Δ, P_1, P_2 and P_3) and regular intensity (m_{00}).

$$Vis = \frac{I_{max} - I_{min}}{I_{max} + I_{min}} \tag{8}$$

Obtained values are included in Table 1. As expected, visibility values of depolarizing metrics are way higher than the displayed from regular intensity image. When comparing P_Δ with IPPs response, the enhancement on image contrast related to IPPS, qualitatively pointed out in the above-stated analysis, is here bolstered: the highest value for ROI 1 (vertical red line) is achieved by P_2 (0.43) which doubles the 0.21 value related to P_Δ (in particular, P_2 increases the visibility by 0.22 units). Furthermore, at ROI 2 (horizontal red line) visibility reaches its highest value at P_1 (0.67): with respect to the standard depolarizing metric P_Δ (0.41), it represents an increment of 63% of image contrast.

Regarding both the qualitative and quantitative analysis of image contrast and biological structures revelation we state the following: IPPs improve the overall sample visualization with respect to other enpolarizing parameters. Particularly, in this study, the highest image contrast is achieved by P_1 and P_2 indices, meanwhile the revelation of hidden tissue structures occurs at P_3.

	ROI 1					ROI 2				
	$\mathbf{m_{00}}$	$\boldsymbol{P_\Delta}$	$\boldsymbol{P_1}$	$\boldsymbol{P_2}$	$\boldsymbol{P_3}$	$\mathbf{m_{00}}$	$\boldsymbol{P_\Delta}$	$\boldsymbol{P_1}$	$\boldsymbol{P_2}$	$\boldsymbol{P_3}$
Vis	0,13	0,22	0,36	0,43	0,28	0,11	0,41	0,67	0,51	0,25

Table 1. Visibility values of intensity (m_{00}) and depolarizing metrics (P_Δ, P_1, P_2 and P_3) images corresponding to two regions of interest: vertical (ROI 1) and horizontal (ROI 2) red lines on Fig. 2 (c).

Considering the dependence of image contrast and hidden structures unfold with different IPPs we perform a joint analysis by means of two pseudo-colored image approaches. This representation shows the different depolarizing mechanisms inherent to the variated biological structures as a weighted linear combination of IPPs: each index is associated with its particular weight and a primary color (red, green or blue). We encode the polarimetric purity indices in two different equations (Eqs. 9 and 10), where the first, second and third terms encode red, green and blue colors, respectively:

$$C_{pix}(x,y) = \alpha_1 P_1(x,y)_R + \alpha_2 P_2(x,y)_G + \alpha_3 P_3(x,y)_B \tag{9}$$

$$C_{pix}(x,y) = \alpha_1 \left[\frac{P_1(x,y) + P_2(x,y) + P_3(x,y)}{3} \right]_R + \alpha_2 \left[\frac{P_2(x,y) + P_3(x,y)}{2} \right]_G + \alpha_3 P_3(x,y)_B \tag{10}$$

where subscripts R, G, B, denote for the red, green and blue channels. The pseudo-colored images are composed by three primary color layers (RGB): each layer pixel values range from 0 to 1 (as IPPs do). The main advantage of pseudo-colored treatment is that we can customize the weight of each purity component, and so the information they provide, by redefining α_i (i=1,2,3) and find a combination which enhances the overall image contrast, or the contrast of some specific structure. We perform the analysis for Eq. (9) and its tailored form (Eq. 10), which are labeled as "Pseudocolored #1" and "Pseudocolored #2", respectively. Obtained images are shown in Fig. 4.

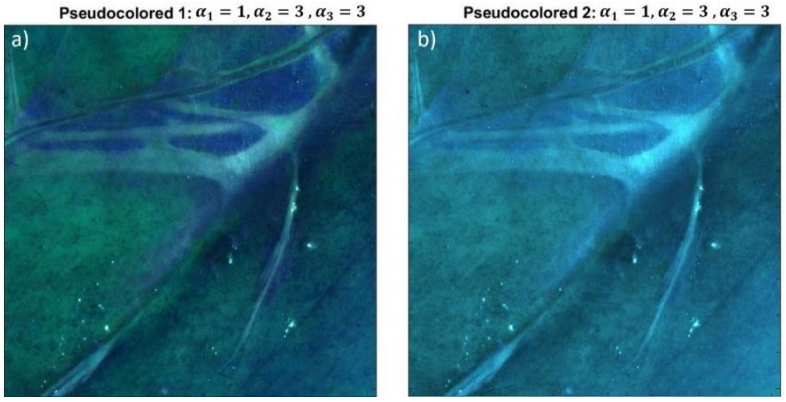

Figure 4. Pseudo-colored approach. (a) Pseudo-colored #1 ($\alpha_1 = 1, \alpha_2 = 3, \alpha_3 = 3$) and (b) Tailored pseudo-colored #2 ($\alpha_1 = 1, \alpha_2 = 3, \alpha_3 = 3$).

Both muscle representations in Fig. 4 (a) and (b) corresponds to the use of Eq. 9 and Eq. 10, respectively, with weights $\alpha_1 = 1$, $\alpha_2 = 3$ and $\alpha_3 = 3$. Because the different colors unwrap the different underlying depolarizing mechanisms of the corresponding biological structures, we customize the weight by enhancing P_2 and P_3 (green and blue layers) instead of P_1 (red) in accordance with the structure revelation results obtained in Fig. 3: this pseudo-colored representation clearly enhances the overall image contrast and unveils the different biological tissue structures. We highlight the suitability of using this approach when revelation of hidden structures or high contrast images are wanted.

4.2 IPPs-based contrast enhancement in *Epipremnum aureum* leaf images

A discussion of the obtained results from an *Epipremnum aureum* leaf analysis is provided down below. The MM of the leaf is obtained at transmission configuration by illuminating at 530 nm. A region of interest (ROI) of 1024×1024 pixels (2.2×2.2 cm^2) is selected from the whole sample. As in the case of animal tissues, the output images from MM-metrics

extraction (IPPs, R, D, and P_Δ) reveal the small contribution of diattenuation, D image and thus, it is not included in the study. Regular intensity image, m_{00}, of *Epipremnum aureum* leaf is shown in Fig. 5 (a). Standard MM-metrics (retardance R and depolarizing index P_Δ) images are given in Fig. 5 (b) and Fig. 5 (c), respectively.

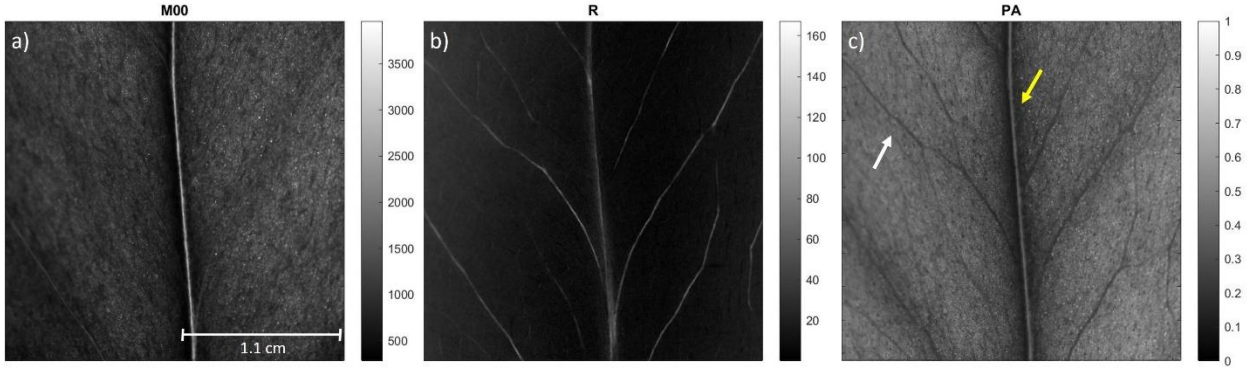

Figure 5. Standard MM-metrics extraction for polarimetric analysis of an *Epipremnum aureum* leaf. (a) Regular intensity image (m_{00}); (b) total retardance, R and (c) depolarization index, P_Δ. Yellow and white arrows indicate principal and secondary veins, respectively.

By inspection it is clearly seen how retardance response is significantly spatial-dependent. Leaf vascular tissue is composed by highly oriented cellulose-I fibrils. These straight chain polymers form crystalline microfibrils which stretch along the direction of large structures. Due to this strong orientation, vascular webs induce birefringence as a consequence of high anisotropic behavior of aligned cellulose polymers. In addition, when looking at depolarization content (Fig. 5 (c)), secondary vascular webs (white arrow) response is more depolarizing (low P_Δ values) than principal vein (yellow arrow): we can assume that the scattering units present on secondary veins are different from those in principal vein and leaf blade (or lamina) in terms of size and density. In counterpart, leaf blade retardance response is way lower: cell structuration contributes to isotropically scatter light in all directions while maintaining the incident polarization state (high P_Δ values). This strong structural difference between vascular webs and blade leads to an enhance of image contrast when polarimetrically analyzing the sample.

To properly decode depolarization information, we analyze the behavior of isolated P_1, P_2 and P_3. Obtained results are presented in Fig. 6.

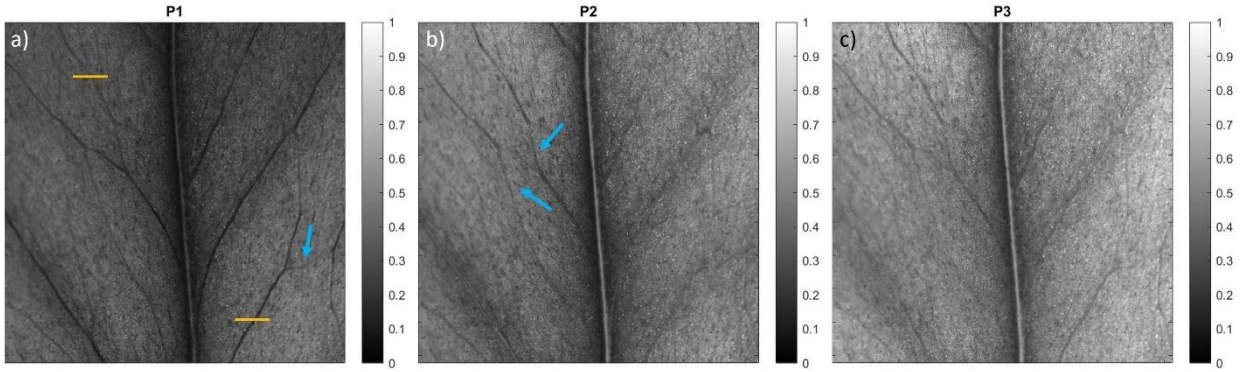

Figure 6. Indices of polarimetric purity images of an *Epipremnum aureum* leaf. (a) P_1; (b) P_2 and (c) P_3. Blue arrows indicate revealed vascular structures. Orange lines correspond to two object of study regions of interest.

The IPPs response with respect to standard depolarization metrics in Fig. 5 is translated into an overall image contrast clearly seen for P_1 (Fig. 6 (a)) and vascular structure revelation (blue arrows in Fig. 6 (a) and (b)) mainly provided by P_1 and P_2 indices. In counterpart, P_3 focuses on enhancing leaf principal vein. In this particular case, the strongly magnification of vascular webs contrast in P_1 and structure revelation characteristics of both P_1 and P_2 points out the suitability of the study of IPPs when looking for depolarization capability of biological tissues.

To supplement the qualitative discussion, we compute the visibility (Eq. (8)) of the two orange-lined regions of interest (1×70 pixel) on Fig. 6 (a). Obtained values are included in Table 2.

	ROI 1					ROI 2				
	$\mathbf{m_{00}}$	$\boldsymbol{P_\Delta}$	$\boldsymbol{P_1}$	$\boldsymbol{P_2}$	$\boldsymbol{P_3}$	$\mathbf{m_{00}}$	$\boldsymbol{P_\Delta}$	$\boldsymbol{P_1}$	$\boldsymbol{P_2}$	$\boldsymbol{P_3}$
Vis	0,27	0,37	0,34	0,44	0,35	0,23	0,33	0,50	0,25	0,27

Table 2. Visibility values of intensity (m_{00}) and depolarizing metrics (P_Δ, P_1, P_2 and P_3) images corresponding to two regions of interest: ROI 1 (located on upper left corner) and ROI 2 (located on lower right corner) orange lines on Fig. 6 (a).

As expected, the visibility values of depolarizing metrics are higher than regular intensity image. Particularly, the qualitatively analysis previously discussed coincides with the visibility obtained for P_Δ and IPPs: the highest visibility value is achieved by P_1 (0.50 at ROI 2) which, in turn, represents an image contrast increment of 51% with respect to P_Δ. Regarding ROI 1, the visibility value provided by P_2 is traduced as an increase of 19% of P_Δ contrast. With this, both the qualitative and quantitative inspection of an *Epipremnum aureum* leaf conclude that IPPs (particularly, P_1 and P_2) are capable to enhance the overall image contrast and reveal vascular structures unable to be seen in regular MM-metrics.

To conclude, we perform a joint IPP analysis, by means of two pseudo-colored image equations, Eq. (9) and (11), labeled as "Pseudo-colored #1" and "Pseudo-colored #3", respectively:

$$C_{pix}(x,y) = \alpha_1[P_2(x,y) - P_1(x,y)]_R + \alpha_2[P_3(x,y) - P_2(x,y)]_G + \alpha_3 P_3(x,y)_B \tag{11}$$

By correctly weighting the polarimetric purity indices liable of enhancing overall vascular structures contrast, we obtain Fig. 7 images.

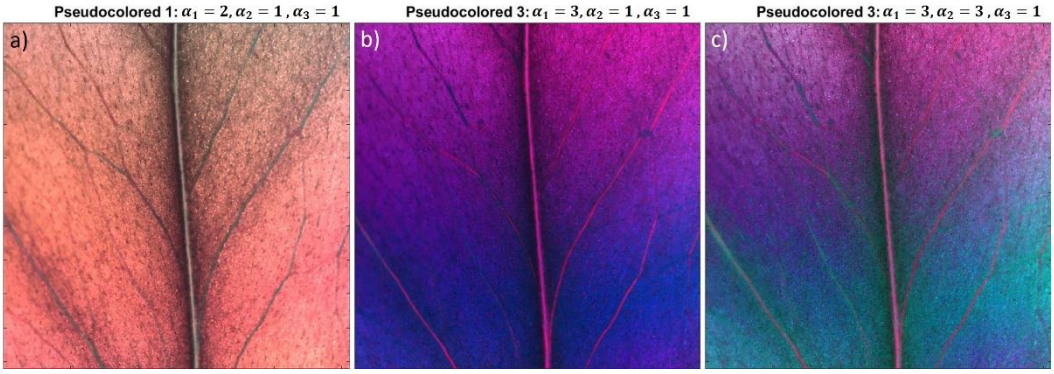

Figure 7. Pseudo-colored approach. (a) Pseudo-colored #1 ($\alpha_1 = 2, \alpha_2 = 1, \alpha_3 = 1$); (b) Pseudo-colored #3 ($\alpha_1 = 3, \alpha_2 = 1, \alpha_3 = 1$) and (c) Pseudo-colored #3 ($\alpha_1 = 3, \alpha_2 = 3, \alpha_3 = 1$).

Leaf representation in Fig. 7 (a) corresponds to the use of Eq. 9 with weights $\alpha_1 = 2$, $\alpha_2 = 1$ and $\alpha_3 = 1$. By adding extra weight to red layer (P_1), we enhance an overall image contrast and unveil vascular structures. The use of Eq. 10 with $\alpha_1 = 3$, $\alpha_2 = 1$ and $\alpha_3 = 1$ and $\alpha_1 = 3$, $\alpha_2 = 3$ and $\alpha_3 = 1$ is presented in Fig. 7 (b) and (c), respectively. By giving larger weight to the subtractions $P_2 - P_1$ and $P_3 - P_2$ we enhance the excess of one purity index with respect to the other which may lead to a larger contrast between different biological structures: vascular or leaf blade. Blue zones on Fig. 7 (b) indicate the high influence of the third term (P_3), meanwhile pink ones show the excess of first and second term subtractions ($P_2 - P_1$ and $P_3 - P_2$) leading and enhance on image contrast of small vascular structures at upper-left corner. In counterpart, green zones on Fig. 7 (c) show the high influence of the second term ($P_3 - P_2$). Different colors, and so different IPPs response, can be related with structural differences of sample such as thickness or density variations, lack or excess of intracellular water presence, etc.

5. CONCLUSIONS

In this proceeding we propose the use of Indices of Polarimetric Purity (IPPs), in front of commonly-used depolarizing indicators, for biological tissues, either animal or vegetal, physical properties inspection. We demonstrate the suitability of this indices by parallel studying the depolarizing response of an *ex-vivo* muscle sample and an *Epipremnum aureum* leaf: both inspections result on an enhance of image contrast and revelation of hidden vascular structures when decoding depolarization information in terms of isolated IPPs. We point out how depolarization, because of the different ways the light scatters when interacting with particular structures of samples, allow us to distinguish between them. Finally, we also propose a total of three pseudo-colored approaches capable to, by properly adjusting IPPs weight, enhance the overall image contrast by imaging the best characteristics of each index of polarimetric purity. This significant image contrast enhancement has been observed in a larger number of samples: *ex-vivo* chicken soft-tissues (myotendinous junction and tendons) and bones in animal framework and different plant specimens (e.g. *Spathiphyllum* sp.) not included in this work to prevent the proceeding to be excessively long.

To conclude, we highlight the interest and suitability of using isolated and pseudo-colored combinations of IPPs as an easy tool for biological samples visualization and depolarization analysis.

REFERENCES

[1] Azzam, R. M. A., Bashara, N. M., [Ellipsometry and Polarized Light], North-Holland Publishing Company, Amsterdam (1977).

[2] Van Eeckout, A., Lizana, A., Garcia-Caurel, E., Gil, J. J., Sansa, A., Rodríguez, C., Estévez, I., González, E., Escalera, J. C., Moreno, I., and Campos, J., "Polarimetric imaging of biological tissues based on the indices of polarimetric purity," Journal of Biophotonics, e201700189, (2017).

[3] Van Eeckout, A., Lizana, A., Garcia-Caurel, E., Gil, J. J., Ossikovski, R., and Campos, J., "Synthesis and characterization of depolarizing samples based on the indices of polarimetric purity," Opt. Lett. 42(20), 4155-4158 (2017).

[4] Novikova, T., Meglinski, I., Ramella-Roman, J. C., Tuchin, V. V., "Special section on polarized light for biomedical applications," J. Biomed. Opt. 21, 071001 (2016).

[5] Tuchin, V. V., "Polarized light interaction with tissues," J. Biomed. Opt. 21, 071114 (2016).

[6] Anwar, S., Firdous, S., Rehman, A. and Nawaz, M., "Optical diagnostic of breast cancer using Raman, polarimetric and fluorescence spectroscopy," Laser Physics Letters, Volume 12, Number 4, (2015).

[7] Yaroslavsky, A. N., Neel, V, and Anderson, R. R., "Demarcation of nonmelanoma skin cancer margins in thick excisions using multispectral polarized light imaging," J. Investig. Dermatol., 121(2), 259-266, 12880416 (2003).

[8] Backman, V., Gurjar, R., Badizadegan, K., Itzkan, L., Dasari, R. R., Perelman, L. T., "Polarized light scattering spectroscopy for quantitative measurement of epithelial cellular structures in situ," IEEE J. Sel. Topics in Quantum Electron., 5(4), 1019-1026, 13 (1999).

[9] Manhas, S., Vizet, J., Deby, S., Vanel, J. C., Boito, P., Verdier, M., "Demonstration of full 4×4 Mueller polarimetry through an optical fiber for endoscopic applications", Opt. Express, 23(3), 3047 (2015).

[10] Qi, J.,Elson, D. S., "A high definition Mueller polarimetric endoscope for tissue characterization," Sci. Rep. 6, 25953 (2016).

[11] Lizana, A., Van Eeckhout, A., Adamczyk, K., Rodríguez, C., Escalera, J. C., Garcia-Caurel, E., Moreno, I., Campos, J., "Polarization gating based on Mueller matrices," J. Biomed. Opt. 22, 056004 (2017).

[12] Qi, J., Elson, D. S., "Mueller polarimetric imaging for surgical and diagnostic applications: a review," J. Biophotonics 10, 950 (2017).

[13] He, H., He, C., Chang, J., Lv, D., Wu, J., Duan, C., Zhou, Q., Zeng, N., He, Y., Ma, H., "Monitoring microstructural variations of fresh skeletal muscle tissues by Mueller matrix imaging," J. Biophotonics, 10, 664-673 (2017).

[14] Ushenko, Y. A., "Investigation of formation and interrelations of polarization singular structure and Mueller-matrix images of biological tissues and diagnostics of their cancer changes," J. Biomed. Opt. 16, 066006 (2011).

[15] Monstrey, S., Hoeksema, H., Saelens, H., Depuydt, K., Hamdi, M., Van Landuyt, K., "A conservative approach for deep dermal burn wounds using polarised-light therapy," Br. J. Plast. Surg., 55(5), 420–426, (2002).

[16] Vanscheidt, W., "The effect of polarized light on wound healing," Eur. J. Plast. Surg., 24(8), 383– 383, 20 (2002).

[17] Stegmann, W., “Behandlung des Ulcus Cruris mit Polarisiertem Licht”, Phlebologie Proktologie, 14, 96-97 (1985).
[18] Van Eeckout, A., Garcia-Caurel, E., Garnatje, T., Dufort, M., Escalera, J. C., Vidal, J., Gil, J. J., Campos, J. and Lizana, A., “Depolarizing metrics for plant simples imaging,” PLoS ONE, 14(3) (2019).
[19] Curran, P. J., “Polarized visible light as an aid to vegetation classification,” Remote Sens. Environ., 12(6), 491-499 (1982).
[20] Goldstein, D., [Polarized Light], 2nd ed., Marcel Dekker, New York (2003).
[21] Chipman, R. A., [Polarimetry: Handbook of Optics], 2nd ed. McGraw Hill, New York (1995).
[22] Rawer, R., Stork, W., and Müller-Glaser, K. D., “Polarimetric methods for measurement of intra ocular glucose concentration,” Biomed. Tech. 47, 186-8 (2002).
[23] Graham, L., Yitzhaky, Y., and Abdulhalim, I., “Classification of skin moles from optical spectropolarimetric images: a pilot study,” J. Biomed. Opt. 18, 111403 (2013).
[24] Yitzhaky, Y., Graham, L., and Abdulhalim, I., “Analysis of skin moles from optical spectropolarimetric images,” Proc. of SPIE 8856, 88562J-1 (2013).
[25] Vanderbilt, V. C., Grant, L., and Daughtry, C. S. T., “Polarization of light scattered by vegetation,” Proc. the IEEE, 73(6), 1012-1024 (1985).
[26] Rondeaux, G., and Herman, M., “Polarization of light reflected by crop canopies,” Remote Sens. Environ., 38(1), 63-75 (1991).
[27] Kharuk, V. I., and Yegorov, V. V., “Polarimetric Indication of Plant Stress,” Remote Sens. Environ., 33 (1), 35-40, 29, (1990).
[28] Arai, K., and Nishimura, Y., “Polarization model for discrimination of broad and needle shaped leaves and estimation of LAI using polarization measurements,” Adv. Space Res., 44(4), 510-516, 30 (2009).
[29] Vanderbilt, V. C., Daughtry, C. S. T., and Biehl, L. L., “Is there spectral variation in the polarized reflectance of leaves?,” Proc. of SPIE, 9099, 1-6 (2014).
[30] Arai, K., and Nishimura, Y., “Polarization model for discrimination of broad and needle shaped leaves and estimation of LAI using polarization measurements,” Adv. Space Res. 44(4), 510-516 (2009).
[31] Berdyugina, S. V., Kuhn, J. R., Harrington, D. M., Santl-Temkiv, T., and Messersmith, E. J., “Remote sensing of life: polarimetric signatures of photosynthetic pigments as sensitive biomarkers,” Int. J. of Astrobiol., 15(1), 45-56, 37 (2016).
[32] Priestley, J., “Photosynthesis, two centuries after its discovery, in Proceedings of the IInd International Congress on Photosynthesis Research Volume I Primary reactions and electron transport”, Eds. G. Forti, M. Avron and A. Melandri, Springer Science & Business Media, 38 (2012).
[33] Patty, C. H. L., Luo, D. A., Snik, F., Ariese, F., Buma W. J., Loes ten Kate, I., “Imaging linear and circular polarization features in leaves with complete Mueller matrix polarimetry,” Biochimica et Biophysica Acta (BBA)-General Subjects, 1862(6), 1350-1363 (2018).
[34] Fiedorowicz, M., and Chaczatrian, G., “Effect of Illumination with the Visible Polarized and Nonpolarized Light on α-Amylolysis of Starches of Different Botanical Origin,” J. Agric. and Food Chem., 51(26), 7815–7819 (2003).
[35] Kanaka Rao, P. V., and Anjaiah, J., “Polarization Imaging of Coffee Arabica,” Int. J. Adv. Sci. Eng. Technol. (IJASEAT), 1, 13–15 (2017).
[36] Gil, J. J., Correas, J. M., Melero, P. A., Ferreira, C., “Generalized polarization algebra,” Monog. Sem. Mat. G. Galdeano, 31, 161 (2004).
[37] Gil, J. J., “Invariant quantities of a Mueller matrix under rotation and retarder transformations,” J. Opt. Soc. Am. A, 33, 52 (2016).
[38] San Jose, I., Gil, J. J., “Invariant indices of polarimetric purity: generalized indices of purity for nxn covariance matrices,” Opt. Commun., 284, 38 (2011).
[39] Ossikovski, R., and Vizet, J., “Eigenvalue-based depolarization metric spaces for Mueller matrices,” J. Opt. Soc. Am. A, 36, 1173-1186 (2019).
[40] Ossikovski, R., “Canonical for ms of depolarizing Mueller matrices,” J. Opt. Soc. Am. A, 27, 123-130 (2010).
[41] Peinado, A., Lizana, A., Vidal, J., Iemmi, C., and Campos, J., “Optimization and performance criteria of a Stokes polarimeter based on two variable retarders,” Opt. Express, 18, 9815-9830 (2010).
[42] Arce-Diego, J. L., Fanjul-Vélez, F., Samperio-García, D., Pereda-Cubián, D., “Mueller coherency matrix method for contrast image in tissue polarimetry,” Proc. SPIE, 6627, 66271T (2007).

[43] Tuchin, V. V., "Tissue Optics: Light Scattering Methods and Instruments for Medical Diagnosis," SPIE Press, Bellingham (2007).
[44] Ghosh, N., Wood, M. F., Vitkin, I., "Mueller matrix decomposition for extraction of individual polarization parameters from complex turbid media exhibiting multiple scattering, optical activity, and linear birefringence," J. Biomed. Opt., 3, 044036 (2008).
[45] Komatsu, K., Mosekilde, L., Viidik, A., Chiba, M., "Polarized light microscopic analyses of collagen fibers in the rat incisor periodontal ligament in relation to areas, regions, and ages," Anat. Rec., 268, 381–387 (2002).
[46] Twietmeyer, K. M., Chipman, R. A., Elsner, A. E., Zhao, Y., and Van Nasdale, D., "Mueller matrix retinal imager with optimized polarization conditions," Opt. Express, 16, 21339-21354 (2008).
[47] Bueno, J. M., "Measurement of parameters of polarization in the living human eye using image polarimetry," Vision Research,40, 3791-3799 (2000).
[48] Gil, J. J., Ossikovski, R., "Polarized Light and the Mueller Matrix Approach," CRC Press, Boca Raton, FL (2016).
[49] Ossikovski, R., "Differential and product Mueller matrix decompositions: a formal comparison," Opt. Lett., 37, 220 (2012).
[50] Gil, J. J., Bernabéu, E., "Obtainment of the polarizing and retardation parameters of a nondepolarizing optical system from the polar decomposition of its Mueller matrix," Opt. Acta, 33, 185 (1986).
[51] Gil, J. J., "Components of purity of a Mueller matrix," J. Opt. Soc. Am. A, 28, 1578 (2011).
[52] Gil, J. J., "Review on Mueller matrix algebra for the analysis of polarimetric measurements," J. Appl. Remote Sens., 8, 081599 (2014).
[53] Van Eeckout, A., Garcia-Caurel, E., Ossikovski, R., Lizana, A., Rodríguez, C., González-Arnay, E., and Campos, J., "Depolarization metric spaces for biological tissues classification," Journal of Biophotonics, e202000083 (2020).
[54] Van Eeckout, A., Lizana, A., Garcia-Caurel, E., Gil, J. J., Sansa, A., Rodríguez, C., Estévez, I., González, E., Escalera, J. C., Moreno, I., and Campos, J., "Indices of polarimetric purity for biological tissues inspection", Proc. of SPIE, 10497, 104971V (2018).
[55] Mustafa, H. F., Jaafar, M. S., "Comparison of wavelength-dependent penetration depths of lasers in different types of skin in photodynamic therapy," Indian J. Phys., 87, 203 (2013).
[56] Garcia-Caurel, E., Ossikovski, R., Foldyna, M., Pierangelo, A., Drévillon, B., De Martino, A., [Advanced Mueller Ellipsometry Instrumentation and Data Analysis], M. Losurdo, K. Hingerls, Springer-Varlag, Berlin (2013).
[57] Butler, D. L., Grood, E. S., Noyes, F. R., and Zernucke, R. F., "Biomechanics of ligaments and tendons," Exer. Sports Sci. Rev., 6, 125 (1978).
[58] James, R., Kesturu, G., Balian, G., and Chhabra, A. B., "Tendon: biology, biomechanics, repair, growth factors, and evolving treatment options," The Journal of Hand Surgery, 33(1), 102-112 (2008).
[59] Charvet, B., Ruggiero, F., and Le Guellec, D., "The development of the myotendinous junction. A review," Musc. Liga. Tend. J., 2(2), 53 (2012).
[60] Hulmes, D. J., "Building collagen molecules, fibrils and suprafibrillar structures," Journal of Structural Biology, 137(1-2), 2-10 (2002).
[61] Schiaffino, S., and Reggiani, C., "Fiber types in mammalian skeletal muscles," Physiological Reviews, 91(4), 1447-1531 (2011).
[62] Asahara, H., Inui, M., and Lotz, M. K., "Tendons and ligaments: connecting developmental biology to musculoskeletal disease pathogenesis," Journal of Bone and Mineral Research, 32(9), 1773-1782 (2017).